A Metallosupramolecular Octahedron Assembled from Twelve Copper(I) Metal Ions and Six 4,4′-(1,2-Phenylene)bis(3,5-dimethylpyrazol-1-ide) Ligands

Maciej Grzywa,[a] Björn Bredenkötter,[a] Dmytro Denysenko,[a] Sebastian Spirkl,[a] Wojciech Nitek,[b] and Dirk Volkmer*[a]

Abstract. The novel coordination compound $[Cu^{I}_{12}(C_{16}H_{16}N_4)_6]$·8DMAc, (**2**), (DMAc = *N,N*-dimethylacetamide) was prepared in solvothermal or microwave assisted reaction. It contains four metallamacrocyclic trinuclear copper(I) pyrazolate coordination units, which occupy four (opposite) faces of an imaginary metallosupramolecular octahedron. Six (4,4′-(1,2-phenylene)bis(3,5-dimethylpyrazol-1-ide) ligands (L_1^{2-}) are placed at the corners of the octahedron. Crystals of the free ligand H_2L_1 [1,2-bis(3,5-dimethyl-*1H*-pyrazol-4-yl)benzene, (**1**)], and $[Cu^{I}_{12}(C_{16}H_{16}N_4)_6]$·8DMAc (**2**), were characterized by single-crystal X-ray structure analyses. Lingand **1** crystallizes in the monoclinic crystal system, with: a = 9.0118(9), b = 14.0075(11), c = 11.7484(11) Å, β = 104.945(5)°, V = 1432.9(2) Å^3, space group $P2_1/c$ (no. 14). Compound **2** crystallizes in the tetragonal system, with: a = b = 19.506(5), c = 42.888(5) Å, V = 16318(6) Å^3, space group $I4_1/amd$ (no. 141). Compound **2** represents a porous structure, where each metallosupramolecular octahedron encloses a solvent-filled cavity of 889 Å^3 (accounting for 6 DMAc molecules, 21.8 % of the cell volume). The incomplete crystal packing arrangement of adjacent $[Cu^{I}_{12}(C_{16}H_{16}N_4)_6]$ moieties in addition leads to solvent-filled interstitial voids accounting to 8.1 % of the cell volume. Removing solvent molecules in vacuo is accompanied by reversible structural changes, leading to a partial loss of porosity, as revealed by Ar-BET sorption analysis. Compounds **1** and **2** were further characterized by elemental and thermogravimetric analysis, X-ray powder diffraction, FTIR-, UV/Vis- and fluorescence spectroscopy. Preliminary results on the activation of molecular oxygen by compound **2** are presented.

Introduction

Polynuclear coordination compounds, which self-assemble into discrete nano-objects of polyhedral shape, often being referred to as "metal-organic polyhedra" (MOPs), or "coordination cages", are subject to systematic research since the early 1990s.[1] Apart from their intriguing structures, these compounds hold promises for applications in controlled drug release,[2] molecular recognition, or catalysis.[3]

Investigations on polynuclear copper complexes are of particular interest, owing to their structural and functional relation to catalytically active sites present in copper-containing oxidases, such as laccase, tyrosinase, ascorbate, and catechol oxidase, which are involved in enzymatic oxidation reactions.[4] Most notably, methane monooxygenase (MMO), produced by methanotrophic bacteria, mediates the oxidation of methane to methanol at ambient conditions.[5] Until today, there is a lack of suitable catalysts for the selective oxidation of methane to methanol. Current processes for activating the strong C–H bond in methane, (average bond dissociation energy of 104 kcal·mol^{-1}),[6] require high temperature, pressure,[7] and are costly and inefficient. A resource and energy efficient production of methanol would open up the opportunity to use it as an alternative fuel, and as a versatile feedstock for industrial downstream products.[8]

Biologically inspired catalysts aiming to mimic structural and functional aspects of copper-containing enzymes thus bear the potential for wide-ranging synthetic applications in the oxidation of organic intermediates containing non-activated C–H-bonds.[9] Suitably designed polynuclear coordination compounds, therefore, are an attractive target for the development of biologically inspired catalytic systems.

Trinuclear metallamacrocyclic copper(I/II) pyrazolate coordination units have been occasionally investigated in catalytic transformation processes.[10] However, because of the great structural flexibility of this coordination unit, elucidating the putative mechanisms, by which molecular oxygen is activated upon coordination to the central Cu^{I} atoms (either in solution or in the solid state) as yet has remained elusive (Scheme 1).

Experimental challenges arise from the fact that Cu^{I} pyrazolate compounds can form complex mixtures of different oligomers in solution.[11] Moreover, strong inter-metallic $Cu^{I}\cdots Cu^{I}$ interactions are frequently observed in the solid state

* Prof. Dr. D. Volkmer
Fax: +49-821-598-5955
E-Mail: dirk.volkmer@physik.uni-augsburg.de
[a] Chair of Solid State and Materials Chemistry
Institute of Physics, Augsburg University
Universitätsstr. 1
86159 Augsburg, Germany
[b] Faculty of Chemistry
Jagiellonian University
ul. R. Ingardena 3
30–060 Kraków, Poland

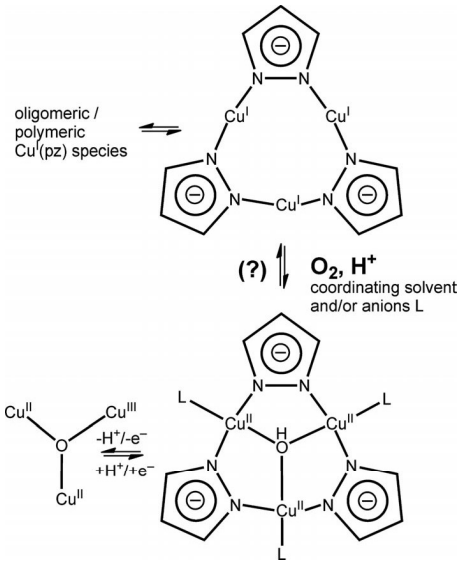

Scheme 1. Representative equilibrium reactions of trinuclear copper pyrazolate coordination units. The proposed redox transformation between tricopper(I) and (II) units was not experimentally confirmed so far. The one-electron oxidation process leading to a mixed-valent Cu^{II}/Cu^{III} species was investigated by cyclic voltammetry.[13]

between adjacent, close packed trimeric Cu^{I} pyrazolate units, leading to variable luminescence properties.[12] These bonding interactions, on the other hand, tend to limit the accessibility of Cu^{I} sites towards reactants, i.e. oxygen.

In order to fully exploit the potential catalytic properties of the trimeric Cu^{I} pyrazolate coordination unit, it will thus be necessary to constrain its arrangement, while maintaining free access to the central copper atoms.

Continuing this line of thought we herein report on a novel dodecanuclear Cu^{I} complex containing six 4,4′-(1,2-phenylene)bis(3,5-dimethylpyrazol-1-ide ligands and four triangular-shaped tricopper(I) pyrazolate cores, thus creating a MOP of roughly octahedral shape (Scheme 2). The resulting compound

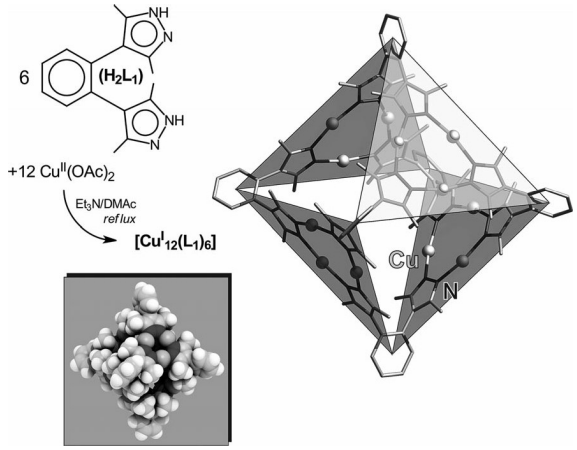

Scheme 2. Formation and (pseudo-)octahedral structure of $[Cu^{I}_{12}(L_1)_6]$ (H_2L_1 = 1,2-bis(3,5-dimethyl-*1H*-pyrazol-4-yl)-benzene) contained in single crystals of **2**. Note that the idealized point group symmetry of the complex is T_d.

was characterized by elemental and thermogravimetric analysis, X-ray powder diffraction, FTIR-, UV/Vis- and fluorescence spectroscopy. Preliminary results on the activation of molecular oxygen by compound **2** are presented.

Results and Discussion

Synthesis and Characterization

The ligand H_2L_1 [1,2-bis(3,5-dimethyl-*1H*-pyrazol-4-yl)benzene] was synthesized according to a previously published procedure.[14] From this, compound **2** was obtained as colorless tetragonal bipyramidal crystals (Figure 1), after heating a DMAc solution of H_2L_1 and copper(II) acetate hydrate in the presence of Et_3N, the latter being required to deprotonate the ligand. Apart from solvothermal synthesis, an alternative approach employing microwave irradiation instead of conventional heating was developed. Microwave syntheses become increasingly popular in the synthesis of organic and inorganic compounds, due to many advantages such as faster reaction times including product precipitation, narrow particle size distributions, enhanced phase purity and product selectivity by reducing unwanted side reactions compared to conventional methods.[15] In the presented case, microwave heating reduced reaction time dramatically, from 3 d to 15 min in conjunction with an increase of product yield.

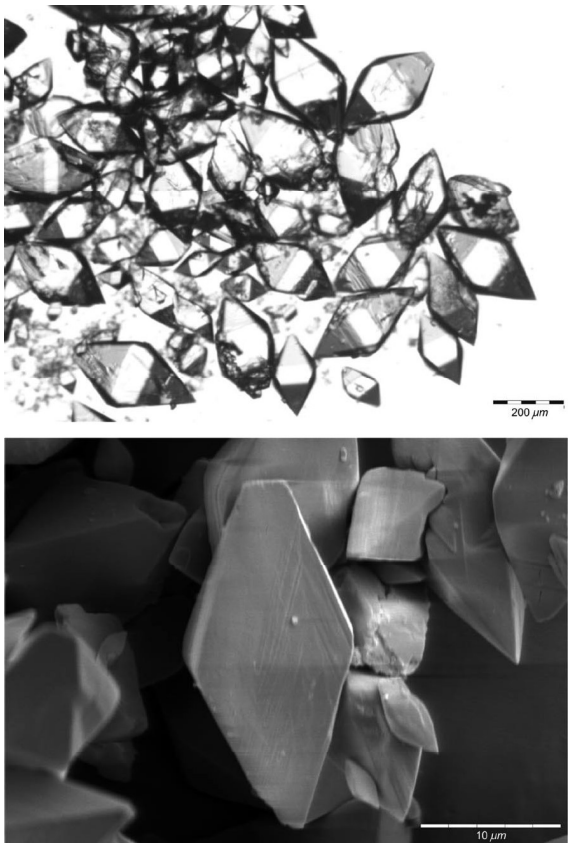

Figure 1. Optical micrograph (upper) and SEM image (below) of single crystals of **2**. Scale bar of the SEM image denotes 10 µm.

Compound **2** is insoluble in H_2O, benzene, acetone, CH_2Cl_2, CH_3CN, 1,4-dioxane, *o*-xylene, 1,2,4-trichlorobenzene, and slightly soluble (at approximate conc. of 1 mg mL^{-1}) in hot chloro-, bromo-, or nitrobenzene, 1,2-dichlorobenzene, or toluene.

Single Crystal Structure Analyses

*Structure Description of 1,2-Bis(3,5-dimethyl-1H-pyrazol-4-yl)benzene (**1**)*

The ligand H_2L_1 (**1**) crystallizes without solvent in the monoclinic crystal system in space group $P2_1/c$ (no. 14). The asymmetric unit contains sixteen carbon and four nitrogen atoms, thus including a single, complete molecule of 1,2-bis(3,5-dimethyl-*1H*-pyrazol-4-yl)-benzene. The pyrazole rings are inclined with respect to each other. The two least-squares planes running through atoms assigned as C7–C9, N1–N2, and C12–C14, N3–N4, respectively, subtend each other at an angle of 65.07(8)°. Compound **1** exhibits a layered structure: The van der Waals interactions between CH_3 groups and hydrogen bonds, running parallel to the crystallographic (100) plane, are responsible for the observed crystal packing motif. The closest non-bonding distance between hydrogen atoms of methyl groups from close-packed molecules is equal to 2.57(1) Å, while N–H···N distances are equal to 2.92(1) Å (N1–H1···N4) and 2.94(2) Å (N3–H3···N2). An Ortep style plot of the asymmetric unit of **1** with atom labels is shown in Figure 2. The packing diagram along the *b* direction of **1** with hydrogen bonds indicated as broken lines is shown in Figure 3. The atomic coordinates and isotropic thermal parameters, selected bond lengths and angles, hydrogen bonds, and additional packing diagrams along *a* and *c* directions for **1** are presented in Tables S1–S3 and Figures S1 and S2 (Supporting Information), respectively.

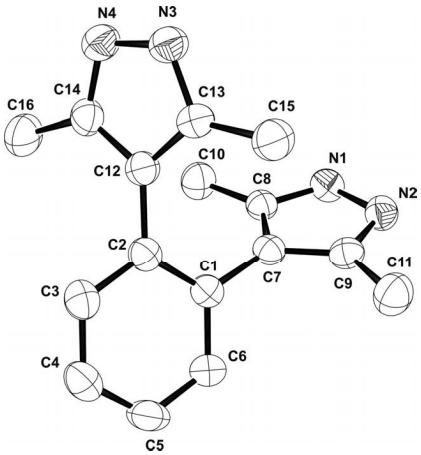

Figure 2. Ortep-style plot of the asymmetric unit of **1**. Thermal ellipsoids probability: 50%. Hydrogen atoms are omitted for clarity.

*Structure Description of $[Cu_{12}(C_{16}H_{16}N_4)_6]\cdot 8$ DMAc (**2**)*

Compound **2** crystallizes in the tetragonal crystal system in space group $I4_1/amd$ (no. 141). The asymmetric unit consists of fourteen carbon, three nitrogen, and two copper atoms, which is 1/8 of the complete octahedrally shaped compound **2**. An Ortep-style plot of the asymmetric unit of **2** with atom labels is shown in Figure 4. The six 4,4′-(1,2-phenylene)-bis(3,5-dimethylpyrazol-1-ide) ligands and four triangular tricopper units form a coordination cage of tetragonal bipyramidal shape (Figure 5). Within each triangular subunit the Cu^I ions are almost linear coordinated by two nitrogen donors belonging to two different ligands [N1–Cu1–N1 and N2–Cu2–N3 angles: 172.9(4)° and 173.6(2)°]. The copper ions are bridged by three pyrazolate rings forming almost planar metallacyclic triangles, which are frequently observed in metal pyrazolates, pyridinates, and amidinates.[16] Two copper atoms [labeled as Cu(2)] involved in intertrimer cuprophilic interactions in each trimer are attracted toward adjacent Cu(2) atoms from neighboring metallamacrocycles, leading to deviation from planarity of the two Cu_3N_6 units (see Figure 6). The Cu(2) atoms are shifted out by 0.085(2) Å from the least-squares plane created by copper and nitrogen atoms from the triangular subunit. Intermolecular Cu···Cu interactions between two neighboring metallamacrocycles are equal at 3.103(5) Å, whereas the distances between copper atoms within triangular units are 3.1499(4) and 3.2728(8) Å, respectively. These values are in a good agreement with those found in structurally related triangular copper compounds.[17,10b] There are two different kinds of micro-pores in the crystal structure. The first type corresponds to confined cavities centered inside each octahedral coordination cage. The second micro-pore is represented by 2-dimensional channels accounting to the interstitial volumes between adjacent coordination units (Figure 7). The pore diameter of the openings leading inside the octahedral coordi-

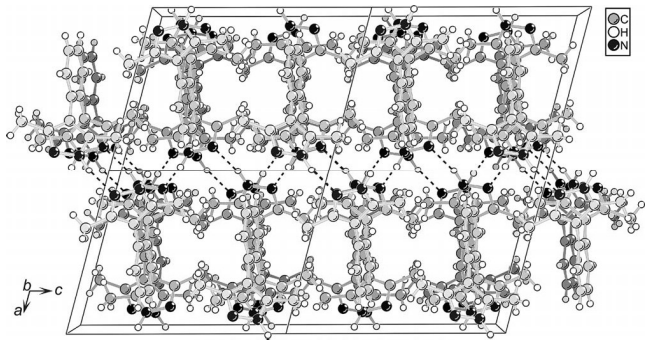

Figure 3. Packing diagram of compound **1** with hydrogen bonds shown as intercepted lines.

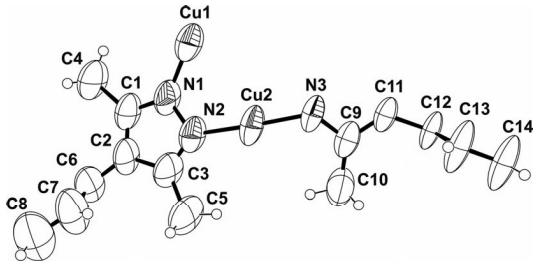

Figure 4. Ortep-style plot of the asymmetric unit of **2**. Thermal ellipsoids probability: 50%.

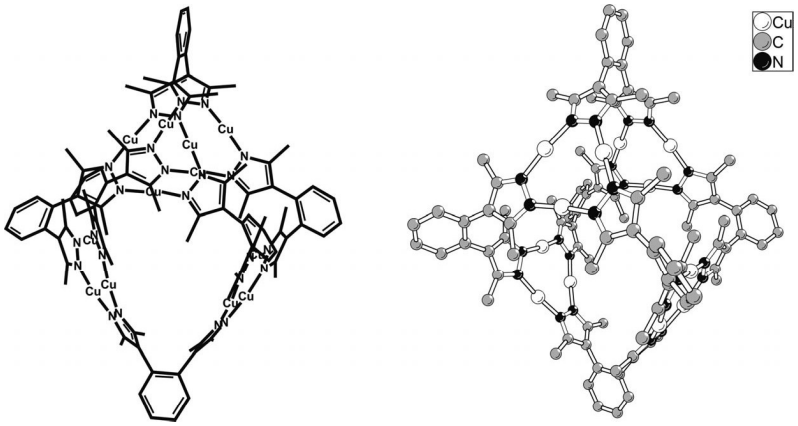

Figure 5. Schematic drawing of the $[Cu^{I}_{12}(L_1)_6]$ coordination unit of compound **2** featuring four fused trinuclear Cu^{I} coordination units, hydrogen atoms are omitted for clarity (left); Ball-and-stick model (right).

nation cages is determined by the cross-sectional distances between hydrogen atoms from methyl groups. Taking the van der Waals radii of hydrogen atoms (1.2 Å) into account, the size of the window is 3.8 Å × 5.3 Å, or 4.6 Å as an average diameter. The 2D hydrophobic channels are flanked by benzene moieties and methyl groups of the ligands. The size of the channel's window is determined by distances between hydrogen atoms from benzene molecules and hydrogen atoms from methyl groups. Taking van der Waals radii of hydrogen atoms (1.2 Å) into account, the approximate diameter of the channels is 10.068 Å. In the crystals of **2** the micro-pores are occupied by disordered solvent molecules, the positions of which were impossible to resolve and refine from the electron density distribution. An estimation with the program PLATON/SQUEEZE[18] reveals that the initial solvent accessible void volume is 7727.1 $Å^3$ (0.495 $cm^3 \cdot g^{-1}$), which is 47.4 % of the unit cell volume [16318(6) $Å^3$] for a probe radius of 1.68 Å, corresponding to the approximate van der Waals radius of argon.[19] For DMAc molecules with an approximate van der Waals radius of 2.9 Å, the value of 4940 $Å^3$ (0.317 $cm^3 \cdot g^{-1}$, 30.3 % of the unit cell volume) is calculated. An alternative geometric pore volume calculation reveals the value of 1329.2 $Å^3$ or 0.085 $cm^3 \cdot g^{-1}$ for the channels, assuming, that these have a cylindrical shape with the diameter of 10.068 Å. For the voids inside the coordination cages, the value of 3556.1 $Å^3$ per unit cell or 0.228 $cm^3 \cdot g^{-1}$ can be obtained, assuming that a sphere with a diameter of 11.93 Å would fit inside this moiety. Thus, for both types of voids, the total pore volume would be 0.313 $cm^3 \cdot g^{-1}$, which is very close to the value obtained with PLATON/SQUEEZE. The calculation of solvent content using the TGA data (Figure 10b) suggests $[Cu_{12}(C_{16}H_{16}N_4)_6] \cdot 8DMAc$ for the composition of **2**, (or 32 DMAc molecules per unit cell), which is consistent with the calculated pore volume (as described in the section about physisorption results). This is also in good agreement with the results from crystal structure analysis. The SQUEEZE procedure gives an electron count of 1231 per unit cell, which corresponds to about 26 DMAc molecules in the unit cell of **2**.

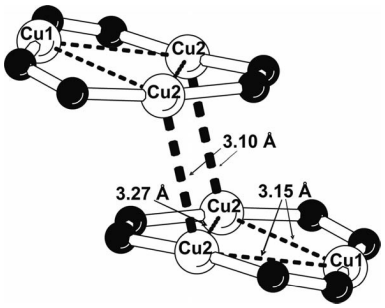

Figure 6. Closest intermetallic distances observed in the crystal structure of **2** between Cu_3N_6 units from neighboring $[Cu^{I}_3(pz)_3]$ metallamacrocycles.

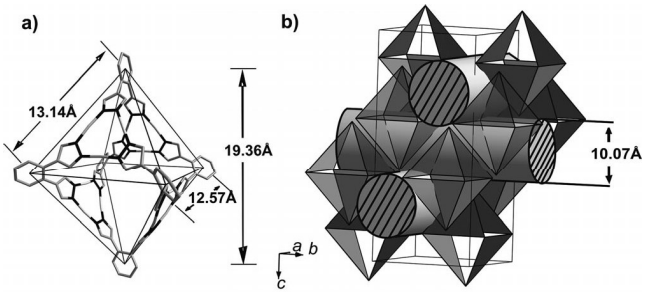

Figure 7. (a) Schematic representation showing the approximate dimensions of $[Cu^{I}_{12}(L_1)_6]$ coordination units in the crystal structure of **2** (CH_3 groups and hydrogen atoms are omitted for clarity); (b) Crystal packing arrangement of $[Cu^{I}_{12}(L_1)_6]$ units in the crystal structure of **2** with interstitial voids fused into open channels.

Schematic representations of the coordination cages and the packing arrangements in the crystal structure of **2** including a sketch of the 2D channels are presented in Figure 7, while a projection of the unit cell is presented in Figure 8.

Selected bond lengths and angles for **2** are presented in Table 1. The atomic coordinates and isotropic thermal parameters, list of bond lengths and angles are collected in the Tables S4 and S5 (Supporting Information), packing diagrams of **2**

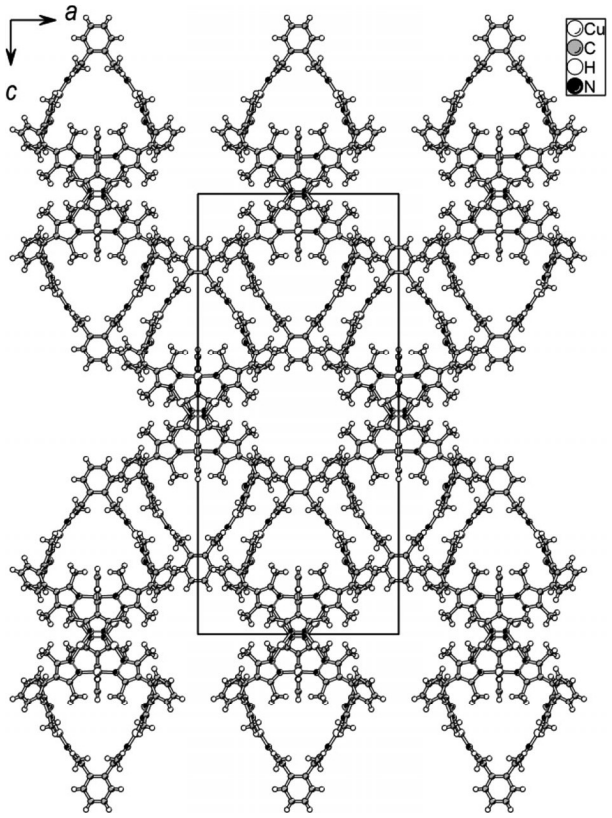

Figure 8. Projection of the unit cell of **2** along the *b* axis (disordered solvent molecules are omitted for clarity).

along *b* and *c* axes are presented in Figures S3 and S4 (Supporting Information), respectively.

Table 1. Selected bond lengths /Å and angles /° in compound **2**.

Cu1–N1a	1.816(5)	N1a–Cu1–N1	173.8(3)
Cu1–N1	1.816(5)	N3–Cu2–N2	173.28(16)
Cu2–N3	1.861(3)	C1–N1–Cu1	132.7(4)
Cu2–N2	1.870(4)	N2–N1–Cu1	120.9(4)
N1–C1	1.349(6)	C3–N2–Cu2	134.4(4)
N1–N2	1.387(5)	N1–N2–Cu2	116.0(4)
N2–C3	1.342(6)	C9–N3–Cu2	131.1(4)
N3–C9	1.352(5)	N3a–N3–Cu2	121.03(11)
N3–N3a	1.355(7)		

Symmetry code: (a) 1 *x*, –*y* + 3/2,*z*.

TGA and XRPD Studies

Phase purity of **2** was confirmed by XRPD measurement at ambient conditions. The experimental XRPD pattern is consistent with the simulated one as gleaned from the single-crystal X-ray diffraction data (Figure 9a,b). Differences in peak intensities are due to occluded solvent molecules. Removal of the solvent by heating the sample at 100 °C in vacuo leads to structural changes (Figure 9c). Interestingly, the intensities of the reflexes are recovered upon immersing the compound in DMAc solvent, which indicates that solvent loss is completely reversible and the initial structure can be completely recovered (Figure 9d). Compound **2** exhibits large "*breathing effects*" upon exposure to different kinds of polar liquids (DMF, DEF, DMAc), whereas non-polar solvents (benzene, naphthalene) are not taken up at all.

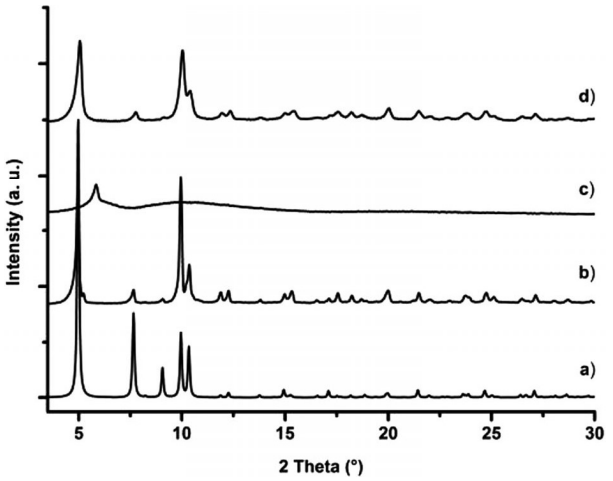

Figure 9. XRPD patterns of **2**: (a) calculated; (b) sample from microwave synthesis; (c) sample heated in vacuo at 100 °C; (d) heated sample after subsequent immersion in DMAc indicating re-constitution of the crystal structure of **2**.

In order to characterize the thermal stability, TGA and variable temperature XRPD experiments were performed exposing the samples to different gas atmospheres (oxygen, nitrogen, air) (Figure 10a,b and Figure 11a,b). The thermogravimetric profile of **2** exhibits a weight loss of –23.07 % between room temperature and 270 °C in nitrogen, and –20.75 % between room temperature and 170 °C in oxygen, which corresponds to the loss of occluded solvent molecules (DMAc). The next degradation steps, in which fractions of the organic ligands are lost, are observed between 400–600 °C in nitrogen and 250–350 °C in oxygen atmosphere, respectively. During the decomposition process in oxygen, a strong exothermic effect is detected. According to the XRPD data, some of the characteristic peaks become weaker and disappear with rising temperature. The most intensive peak at approx. 5° in 2θ, corresponding to the (101) crystal plane, which separates triangular tricopper units from adjacent octahedral $[Cu^{I}_{12}(L_1)_6]$ moieties (see Figure S5, Supporting Information), is observed up to 200 °C. Subsequent heating of the sample leads to partial amorphization, the (101) peak shifts to higher values of 2θ, indicating that the unit cell volume decreases. Compound **2** finally decomposes upon reaching a final temperature of 220–230 °C. In nitrogen atmosphere the formation of Cu_2O and further oxidation of Cu_2O to CuO, due to the presence of residual oxygen, is detected at 350 °C. In air, the formation of CuO from **2** is already observed at 300 °C.

Physisorption Results

Compound **2** exhibits permanent porosity, which is confirmed by argon gas sorption. Prior to sorption measurement, the crystalline sample was suspended and stirred in dichloromethane, leading to solvent exchange of less volatile DMAc

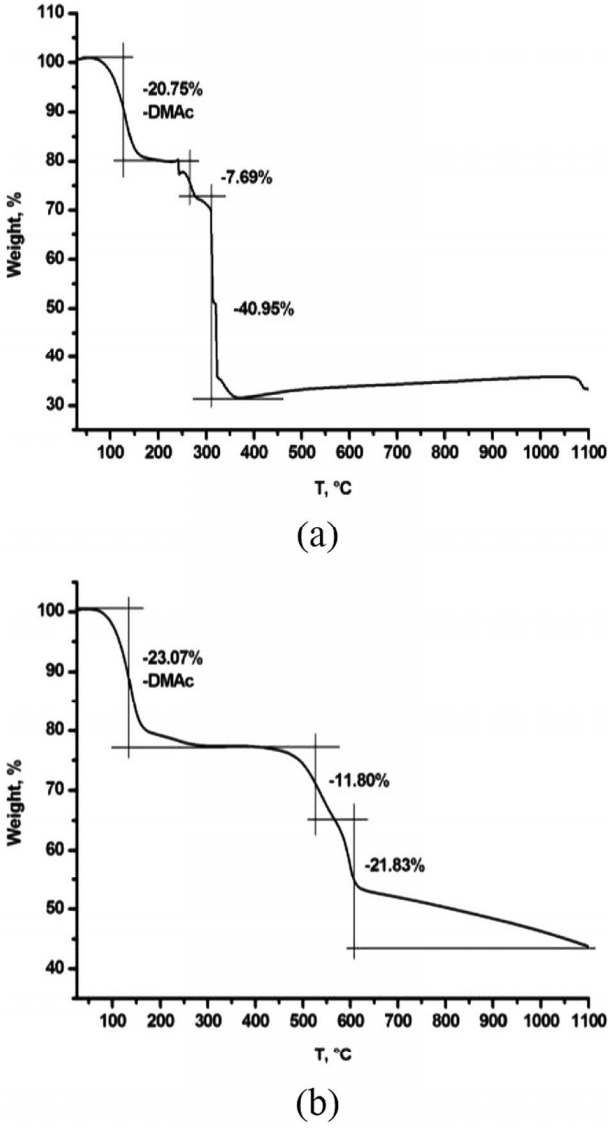

Figure 10. (a) Temperature dependent weight-loss of **2** under flowing oxygen gas. (b) Temperature dependent weight-loss of **2** under flowing nitrogen gas.

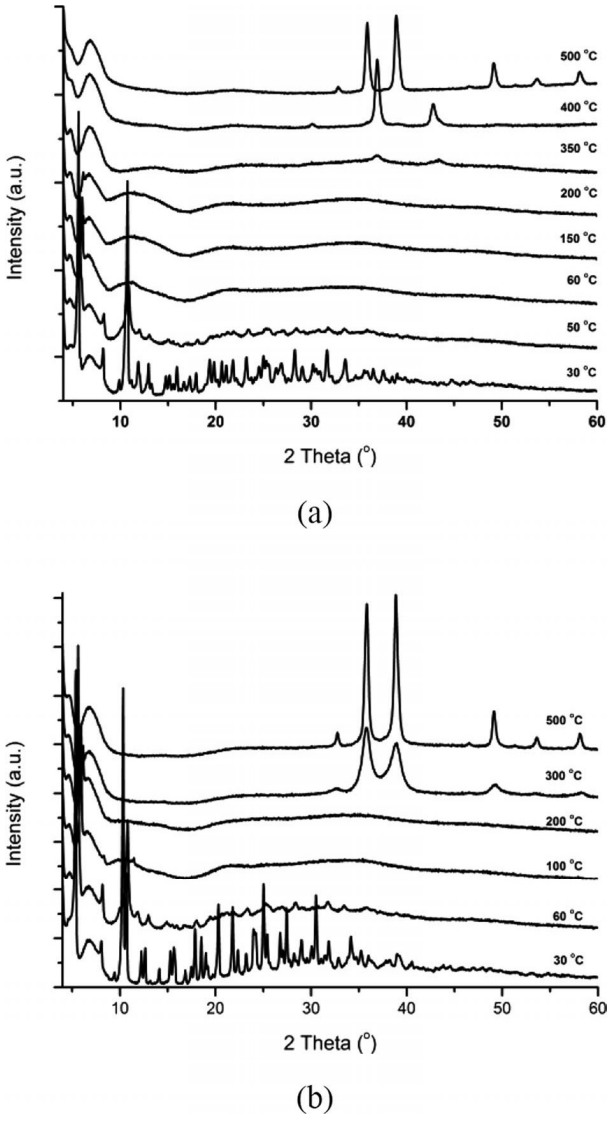

Figure 11. (a) VTXRPD plots of **2** kept in a nitrogen atmosphere, sampled in the temperature range of 30–500 °C. 400 °C – Cu_2O, PDF No. 5–667; 500 °C – CuO, PDF No. 5–661. (b). VTXRPD plots of **2** kept in air, sampled in a temperature range of 30–500 °C. 500 °C – CuO, PDF No. 5–661.

molecules, and then heated at 100 °C in vacuo for 1 h. The argon adsorption isotherm follows type I behavior, typical for micro-porous solids. The maximum uptake achieved at 77 K and p p_0^{-1} = 1 is 306 $cm^3 \cdot g^{-1}$ (Figure 12). The observed small hysteresis indicates dynamic structural changes during the adsorption and desorption processes. The micro-pore volume obtained from the sorption isotherm is 0.336 $cm^3 \cdot g^{-1}$ applying the NLDFT method.[20] The same value was obtained by using de Boer *t*-method micro-pore analysis.[21] This value is considerably lower than calculated by PLATON/SQUEEZE for argon (0.495 $cm^3 \cdot g^{-1}$), which could be due to the structural changes described above. Interestingly, an estimation of the pore volume using the solvent content obtained from TGA analysis (23.07 %), assuming that the density of DMAc in micro-pores is equal to its density in the bulk state (0.937 $g \cdot cm^{-3}$), reveals a value of 0.32 $cm^3 \cdot g^{-1}$, which is very close to the value predicted by PLATON/SQUEEZE for DMAc molecules (0.317 $cm^3 \cdot g^{-1}$) filling the void volume of **2**. This indicates that the crystal structure of **2** can be completely recovered upon adsorption of polar molecules such as DMAc.

Fitting adsorption data into the BET equation gives a surface area of 680 $m^2 \cdot g^{-1}$. To evaluate the pore size distribution, the argon sorption isotherms sampled at 77 K were analyzed using non-local density functional theory (NLDFT) implementing a carbon equilibrium transition kernel for argon adsorption at 77 K based on a slit-pore model.[22] The distribution calculated by fitting the sorption data reveals several maxima, reflecting the intricate structure of voids in the crystal structure of **2** (Figure 13). This distribution cannot be easily rationalized in terms of porosity analysis based on the crystal structure of **2**, which contains occluded DMAc solvent molecules. Thus, two main

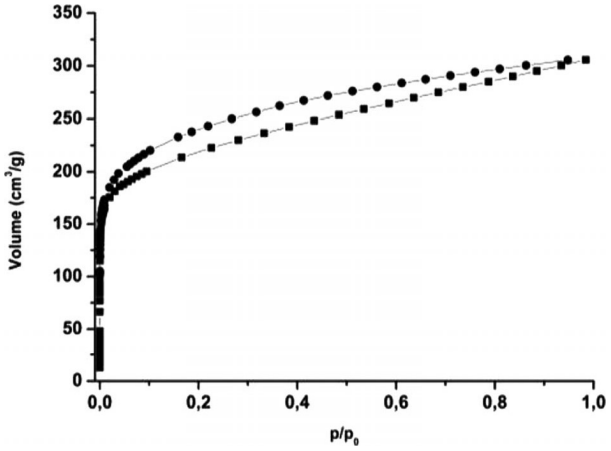

Figure 12. Argon adsorption (squares) and desorption (circles) isotherms measured for desolvated sample of **2** at 77K.

types of micro-pores with diameters of 5.0 and 8.0 Å, respectively, are detected experimentally, which are smaller than the channel / void model derived from crystallographic data. In order to enhance the permanent porosity of compound **2**, supercritical drying[23] and freeze-drying[24] procedures were tested. Unfortunately, both techniques did not exert any influence on the experimentally determined surface area of compound **2**.

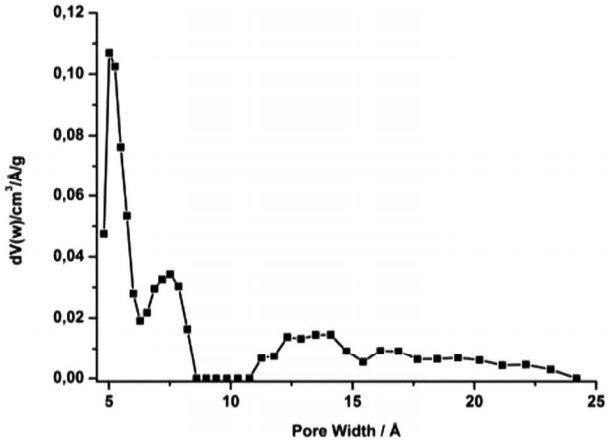

Figure 13. Pore size distribution for **2** calculated by fitting NLDFT model to the argon sorption data.

Fluorescence Spectroscopy Studies

Trinuclear closed-shell d^{10} (Au^I, Ag^I, Cu^I) complexes have been utilized as luminescent materials.[12a] As expected, the presence of luminophoric Cu_3 units in compound **2** results in photoluminescence at room temperature. As shown in Figure 14, compound **2** exhibits a broad emission band in the visible region with a maximum at 545 nm (c-line) upon excitation at a wavelength of 301 nm (a-line). This band is assigned to metal-based phosphorescence and it is in good agreement with the data of structurally related trinuclear Cu^I pyrazolate compounds [e.g. 542 nm for $[Cu(pz)]_3$)].[25] For these type of compounds it is well known, that the photoluminescence properties depend on the Cu···Cu distance,[26] which must be smaller or close to twice the van der Waals radius of Cu^I (1.4 Å) in order to achieve low-energy emission. In the case of compound **2**, the *intra*trimeric Cu···Cu distance of 3.15–3.27 Å is considerably larger than 2.8 Å and would normally not lead to a large red shift of the emission band. The red shift found for compound **2**, as compared to a free ligand **1**, can be explained by structural changes upon solvent loss. Thus, the shortest *inter*-trimeric Cu···Cu distance is 3.10 Å in the intact crystals of **2** (see Figure 6), which is expected to decrease upon solvent removal due to cuprophilic interactions. Such structural confinement of flexible Cu_3-containing complexes leading to specific fluorescence properties has been described previously in the literature.[27] Compound **1** exhibits two fluorescence bands with significant shifts at 431 and 470 nm (a-line) upon excitation at a wavelength at 301 nm. These bands, which could be assigned to the intraligand π–π* transitions in 1,2-bis(3,5-dimethyl-*1H*-pyrazol-4-yl)benzene disappear in the spectrum of compound **2**.

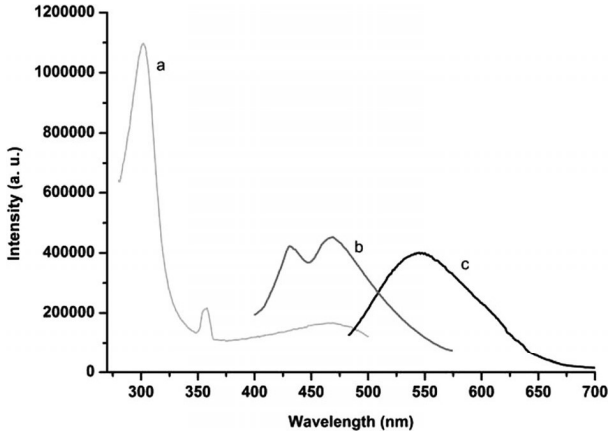

Figure 14. Solid-state photoluminescence spectra for **1** and **2** at room temperature. (a)-line – excitation spectrum, (b)-line – compound **1**, (c)-line – compound **2**.

The solid-state UV/Vis spectrum of the free ligand **1** displays one absorption peak at 280 nm in the UV region, as depicted in Figure 15. This band can be assigned to ligand-centered π→π* transitions of **1**. Compound **2** exhibits the same strong band at 280 nm (Figure 15, b-line). Due to very low room-temperature solubility of **2** in common solvents, it was not possible to record UV/Vis spectra from solution.

UV/Vis Spectroscopy and Reactivity Studies

In order to probe the reactivity of **2** towards molecular oxygen, the sample was oxidized by keeping it in air for 15 h and, alternatively, by adding *tert*-butylhydroperoxide (see Figure S6, Supporting Information). In both cases the color of the samples changed from colorless to green and a new band appeared in the UV/Vis spectrum at ca. 650 nm, typical for d-d transitions in Cu^{2+} ions.[28] Moreover, the shape of the crystals after the oxidation with *t*BuOOH was not changed. In addition, a strong metal-to-ligand charge-transfer band at 345 nm ap-

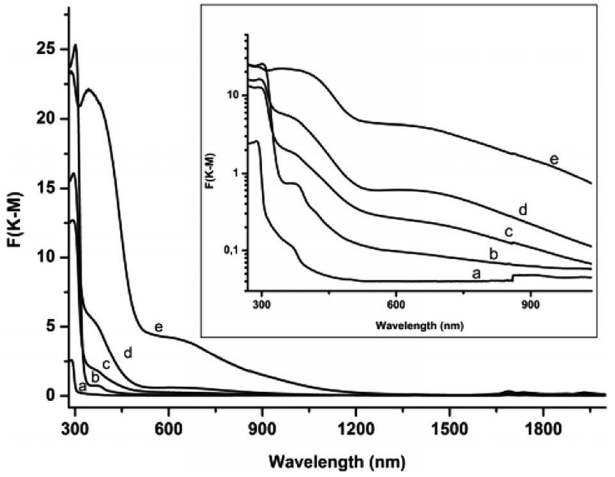

Figure 15. UV/Vis spectra of **1** and **2** at room temperature. (a)-line: **1**; (b)-line: **2**; (c)-line: **2** dried in high-vacuum; (d)-line: **2** after 15 h exposure to air; (e)-line: **2** oxidized by *t*BuOOH.

pears (Figure 15). It is also possible to oxidize the sample by bubbling pure oxygen gas through a suspension of the sample in NMP (1-methyl-2-pyrrolidone). It is worth to mention, that the oxidized green sample can be fully reduced upon prolonged heating (3–5 h) in DMF at 120 °C, during which time the color of the sample changes from green to off-white. XRPD measurements indicate that the structure remains stable during oxidation and reduction reactions (see Figure S8).

For preliminary studies of possible oxidation/reduction processes of **2** TPO/TPR techniques were implemented. These investigations were carried out with a pulse chemisorption analyzer coupled with a quadrupole mass spectrometer using calibrated gas mixtures containing 5 vol% of O_2/He and 5 vol% of CO/He for oxidation and reduction cycles, respectively. The detailed description of the calibration process is presented in the Supporting Information. A heating rate of 10 K·min^{-1} was employed and the experiments were carried out in the temperature ranges of 25–150 °C. The decrease of O_2 content was monitored with a thermal conductivity detector TCD, CO_2 formed during the reduction of the oxidized species was detected by mass spectrometry (MS). Prior to measurements, the sample of **2** was subjected to high-vacuum at 100 °C over a period of 2 h. Two series of TPO profiles were recorded for **2** (three and two cycles, see Figure 16). After the first series (three cycles of TPR/TPO) the XRPD pattern of the oxidized species was collected (Figure S8). Next, the sample was immersed in DMF and heated for 5 h (XRPD pattern was collected). Prior to the second series of TPO/TPR (two cycles), the sample again was subjected to high-vacuum at 100 °C for 2 h.

The obtained TPO data are presented in Table S6 (Supporting Information). TPO/TPR studies show in the first cycle an oxygen uptake of 4.65×10^{-2} (± 2%) mmol per 1 mmol of Cu_3 units. After reduction with CO, the uptake of oxygen decreases to 3.16×10^{-2} (± 2%) mmol per 1 mmol of Cu_3 units, which equals the value obtained in the third cycle. The low amount of chemically bound oxygen is probably due to the positional rearrangement of $[Cu^{I}_{12}(L_1)_6]$ coordination units in the crystal lattice of **2** upon solvent loss, leading to a limited accessibility of central copper atoms.

The XRPD pattern after oxidation and reduction cycles followed by treatment with hot DMF is similar to the initial one calculated on the basis of single crystal data of **2** (see Figure S8). This indicates that the oxidation/reduction sequences of Cu^{I} to Cu^{II} are reversible and take place without collapse of the structure. Unfortunately all attempts to collect X-ray diffraction data of oxidized single crystals of **2** as yet have failed in our hand, which is ascribed to the very weak scattering of the oxidized form of the crystals.

Conclusions

The work focuses on the synthesis and characterization of a novel supramolecular complex assembled from trinuclear Cu^{I} units and tetradentate 4,4′-(1,2-phenylene)bis(3,5-dimethylpyrazol-1-ide ligands leading to coordination cages of octahedral arrangement. The compound remains porous after sol-

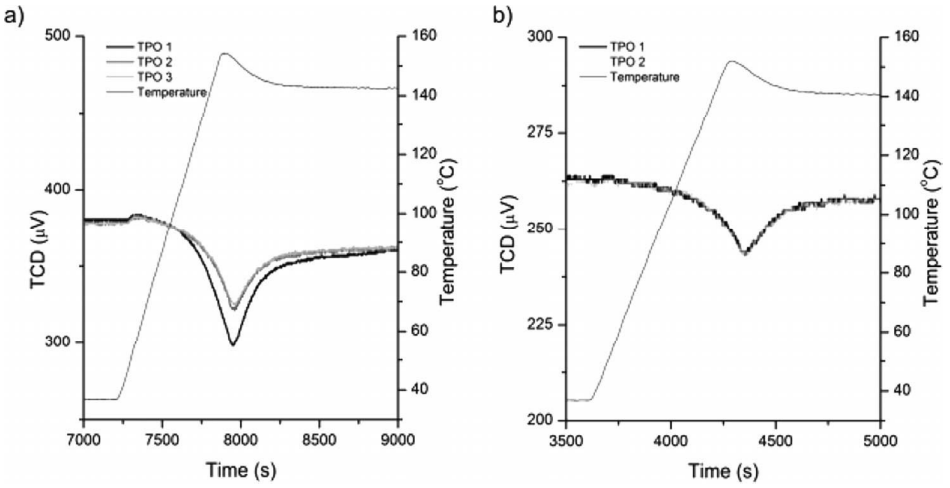

Figure 16. TPO/TPR studies of **2**. (a) first series of TPO/TPR cycles 1–3; (b) second series of TPO/TPR cycles 5–6.

vent removal, as confirmed by gas sorption. Preliminary reactivity studies of **2** exposed to molecular oxygen and *t*BuOOH show that this compound is stable in the solid state during repeated oxidation and subsequent reduction of the copper ions. The fact that compound **2** can be re-crystallized from non-coordinating solvents such as chlorobenzene, furnishing single crystals of identical shapes indicates that the $[Cu^{I}_{12}(L_1)_6]$ coordination cages should remain intact in solution. Since **2** can be reversibly oxidized and reduced if exposed to a reactive gas atmosphere it should represent a potential catalyst for performing oxidation reactions. A screening for catalytic reactions such as oxidation of hydrocarbons shown by porous coordination compounds containing trinuclear copper pyrazolate metallacycles such as **2** (and structurally related compounds) will be reported elsewhere.

Experimental Section

Materials and General Methods: All starting materials were of reagent grade and used as received from the commercial supplier. Fourier transform infrared (FTIR) spectra were recorded with ATR in the range 4000–400 cm^{-1} with a Bruker Equinox 55 FT-IR spectrometer. The following indications are used to characterize absorption bands: very strong (vs), strong (s), medium (m), weak (w). Elemental analyses (C, H, N) were carried out with a Perkin-Elmer 2400 Elemental Analyzer. Thermogravimetric analysis (TGA) was performed with a TGA/SDTA851 Mettler Toledo analyzer in a temperature range of 25–1100 °C in flowing nitrogen and oxygen at a heating rate of 10 °C·min^{-1}. Ambient temperature X-ray powder diffraction (XRPD) patterns were measured with a PANalytical X′Pert PRO diffractometer with X′Celerator detector operated at 45 kV, 40 mA, Cu-K_α (λ = 1.54178 Å) with a scan speed of 98.58 s per step and a step size of 0.033 in 2θ. Variable temperature X-ray powder diffraction (VTXRD) measurements were performed in air and nitrogen atmosphere in a temperature range from 30 to 500 °C with the same diffractometer equipped with an Anton Paar HTK 1200N reaction chamber. Temperature program between measurements: heating rate, then 10 min isotherm. The patterns were recorded in the 4–60°2θ range, with time 98.6 s per step, and a step 0.033° 2θ. The argon sorption isotherms at –196 °C up to p-p_0^{-1} = 1 were measured with a Quantachrome Autosorb-1C apparatus. High purity gas was used for the adsorption experiments (argon 99.999 %). Luminescence spectra were acquired with a FS920 spectrofluorometer (Edinburgh Instruments) equipped with a TMS300 monochromator, S900 single photon photomultiplier, Xe900 450W Xenon arc lamp at room temperature. The excitation and emission spectra were corrected for the wavelength-dependent lamp intensity and detector response, respectively. UV/Vis spectra were recorded with a Perkin-Elmer Lambda 750S spectrometer in the range of 250–2000 nm with a lamp change at 320 nm. TPO/TPR measurements were carried out with a BELCAT-B (Bel. Inc. Japan) instrument coupled with a quadrupole mass spectrometer.

Synthesis of 1,2-Bis(3,5-dimethyl-*1H*-pyrazol-4-yl)benzene (1): 1,2-Bis(3,5-dimethyl-*1H*-pyrazol-4-yl)benzene was synthesized according to the published procedure.[14] Soluble in: DMF, DEF, DMAc, 1,4-dioxane, DMSO, hot MeOH, EtOH, insoluble in H_2O, THF, chlorobenzene, nitrobenzene, CH_3CN. **^{1}H NMR** (400 MHz, [D_6]DMSO, 100 °C, ppm): δ = 11.70 (s_{br}, 2H, NH), 7.28–7.30 (A-part, AA'BB'-system, 2H, PhH), 7.19–7.21 (B-part, AA'BB'-system, 2H, PhH), 1.79 (s, 12H, CH_3). **IR** (KBr): $\tilde{\nu}$ = 3495 vw, 3184 s, 3137 s, 3080 s, 3023 s, 2965 s, 2921 s, 1961 w, 1930 w, 1828 w, 1659 w, 1580 s, 1518 s, 1453 s, 1409 vs, 1375 m, 1300 s, 1272 s, 1235 s, 1148 s, 1113 w, 1062 m, 1037 s, 1006 s, 970 s, 8433 s, 775 s, 7512 s, 655 m, 623 m, 588 m, 540 m, 491 m, 418 w cm^{-1}. The ^{1}H-NMR and IR spectra of **1** are shown in Figure S9 and S10 (Supporting Information), respectively.

Syntheses of $[Cu_{12}(C_{16}H_{16}N_4)_6]$ (2), Solvothermal Method: A mixture of $Cu(OAc)_2{\cdot}H_2O$ (11 mg, 0.055 mmol) and 1,2-bis(3,5-dimethyl-*1H*-pyrazol-4-yl)benzene (15 mg, 0.056 mmol) was dissolved in DMAc (4 mL). Et_3N (0.1 mL) was added and the solution was placed in a glass tube (10 mL). The tube was closed with a cap and heated at 120 °C for 3 d and cooled to room temperature. The colorless crystals were filtered off by suction, washed thoroughly with MeOH and stored in a nitrogen atmosphere. The synthesis can be similarly performed at larger quantities (upscale factor: 50). Yield: 8 mg, 74 % (based on $Cu(OAc)_2{\cdot}H_2O$). $C_{16}H_{16}N_4Cu_2$: calcd: C 49.10; H 4.12; N 14.31 %; found: C 49.13; H 5.53; N 14.40 %. **IR** (KBr): $\tilde{\nu}$ = 3447 w, 3048 w, 3011 w, 2914 m, 1744 w, 1648 vs, 1547 m, 1493 s, 1432 s, 1392 s, 1371 s, 1339 m, 1287 m, 1263 m, 1184 m, 1144 m, 1059 w, 1012 s, 809 w, 758 m, 736 w, 704 w, 660 w, 591 m, 572 m, 472 w, 420 w cm^{-1}.

Microwave Irradiation Method: A mixture of $Cu(OAc)_2{\cdot}H_2O$ (11 mg, 0.055 mmol) and 1,2-bis(3,5-dimethyl-*1H*-pyrazol-4-yl)benzene (15 mg, 0.056 mmol) was dissolved in DMAc (4 mL). Et_3N (0.1 mL) was added and the solution was placed in a Pyrex sample tube (10 mL). The tube was closed with a cap and placed in a microwave synthesizer (CEM, Discover S). The resulting mixture was heated to 140 °C at 200 W, kept under these conditions for 15 min and cooled to room temperature. The colorless microcrystalline material was filtered off and washed with MeOH, and stored in a nitrogen atmosphere. Yield: 10 mg, 93 % [based on $Cu(OAc)_2{\cdot}H_2O$]. This material exhibited the same analytical results as the one obtained by the solvothermal method.

Single Crystal X-ray Diffraction of 1,2-Bis(3,5-dimethyl-*1H*-pyrazol-4-yl)benzene (1): X-ray data for the single crystal structure determination were collected with a Kappa CCD Bruker-Nonius diffractometer. The crystal data and the refinement details for the compound **1** are listed in Table 2. The structure was solved by direct methods and refined using SHELXS and SHELXL–97 programs,[29] respectively. Anisotropic displacement parameters were used for all non hydrogen atoms. Hydrogen atoms were added at idealized positions. Hydrogen atoms were given isotropic displacement parameters equal to 1.2 and 1.5 (for methyl groups) times the equivalent isotropic displacement parameter of the atom to which the hydrogen atom is attached.

Single Crystal X-ray Diffraction of $[Cu_{12}(C_{16}H_{16}N_4)_6]{\cdot}$8DMAc (2): Many attempts of obtaining suitable data sets from X-ray diffraction experiments on single crystals of $[Cu_{12}(C_{16}H_{16}N_4)_6]{\cdot}$8DMAc were performed. In three cases we decided to collect the full data for the determination of the crystal structure. To prevent loss of solvent molecules from the crystals, in two cases the single crystals were placed in a capillary in the vapor of the mother liquid, while the third crystal was cooled to 100 K. Unfortunately, in all cases poor-quality data was obtained. Finally, one of the data sets collected from the single crystal measured in a capillary were chosen for further calculations, to obtain the correct crystal model and to perform crystal structure refinement. Diffraction data were collected with an Oxford Diffraction SuperNova four circle diffractometer, equipped with a Mo-K_α (0.71069 Å) radiation source, graphite monochromator and CryoJet system for measurements at low temperature. Cell refinement and data reduction was performed using firmware.[30] The positions of most non-hydrogen atoms were determined by direct methods using SIR-97.[31] All non-hydrogen

Table 2. The crystal data and structure refinement summary for compounds **1** and **2**.

	1	**2**
Empirical formula	$C_{16}H_{18}N_4$	$C_{24}H_{24}Cu_3N_6$
Formula	$C_{16}N_4H_{18}$	$[Cu_{12}(C_{16}H_{16}N_4)_6]$•8DMAc
Mr	266.34	587.11
T /K	293(2)	293(2)
Crystal system	monoclinic	tetragonal
Space group (no)	$P2_1/c$ (14)	$I4_1/amd$ (141)
a /Å	9.0118(9)	19.506(5)
b /Å	14.0075(11)	
c /Å	11.7484(11)	42.888(5)
β /°	104.945(5)	
V /Å^3	1432.9(2)	16318(6)
Z	4	16
D_c /g•cm^{-3}	1.235	0.956
μ /mm^{-1}	0.076	1.564
F(000)	568	4752
θ range /°	2.91–27.52	3.17–26.37
Refls. collected	11243	14929
Refls. unique	3290	4371
$R_{int.}$	0.1221	0.0615
R_1 [$I > 2\sigma(I)$][a)]	0.0586	0.0752
wR_2 (all data)[b)]	0.1568	0.2508
GooF	0.914	0.836
Largest diff. peak and hole /e•Å^{-3}	0.208 and –0.217	1.051 and –0.360

a) $R_1 = \Sigma||F_o|-|F_c||/\Sigma|F_o|$. b) $wR_2 = \Sigma[w(F_o^2-F_c^2)^2]/\Sigma[w(F_o^2)^2]^{1/2}$.

atoms were refined anisotropically using weighted full-matrix least-squares on F^2. All hydrogen atoms were positioned with an idealized geometry and refined using a riding model. Refinement and further calculations were carried out using SHELXL-97.[29] The highest residual electron densities of 1.051 e•Å^{-3} were found in the large cavities of **2**, which were described to the disordered solvent molecules. However, it was not possible to locate these molecules reliably and therefore they were excluded from refinement. The PLATON's SQUEEZE procedure[18] was applied. Selected crystal data and details of structure refinement for **2** are provided in Table 2.

Crystallographic data (excluding structure factors) for the structures in this paper have been deposited with the Cambridge Crystallographic Data Centre, CCDC, 12 Union Road, Cambridge CB21EZ, UK. Copies of the data can be obtained free of charge on quoting the depository numbers CCDC-924903 and CCDC-924904 (Fax: +44-1223-336-033; E-Mail: deposit@ccdc.cam.ac.uk, http://www.ccdc.cam.ac.uk).

Supporting Information (see footnote on the first page of this article): Atomic coordinates, bond lengths and angles, packing diagrams, H NMR, IR spectra, TPO/TPR studies.

Acknowledgements

This work was supported by a grant from the Ministry of Science, Research and Art Baden-Württemberg and by the Deutsche Forschungsgemeinschaft (DFG) within Priority Program "Porous Metal-Organic Frameworks" (SPP 1362, MOFs). The authors thank *Alexandre Santos Abreu* (Institute of Physics, Augsburg University) for performing fluorescence measurements.

References

[1] Selected reviews: a) L. R. MacGillivray, J. L. Atwood, *Angew. Chem. Int. Ed.* **1999**, *38*, 1018; b) M. Fujita, K. Umemoto, M. Yoshizawa, N. Fujita, T. Kusukawa, K. Biradha, *Chem. Commun.* **2001**, 509; c) P. H. Dinolfo, J. T. Hupp, *Chem. Mater.* **2001**, *13*, 3113; d) S. R. Seidel, P. J. Stang, *Acc. Chem. Res.* **2002**, *35*, 972; e) T. D. Hamilton, L. R. MacGillivray, *Cryst. Growth Des.* **2004**, *4*, 419; f) D. J. Tranchemontagne, Z. Ni, M. O'Keeffe, O. M. Yaghi, *Angew. Chem. Int. Ed.* **2008**, *47*, 5136; g) J. J. Perry IV, J. A. Perman, M. J. Zaworotko, *Chem. Soc. Rev.* **2009**, *38*, 1400.

[2] a) M. Tonigold, J. Hitzbleck, S. Bahnmüller, G. Langstein, D. Volkmer, *Dalton Trans.* **2009**, 1363; b) N. P. E. Barry, O. Zava, P. J. Dyson, B. Therrien, *Chem. Eur. J.* **2011**, *17*, 9669.

[3] a) D. Fiedler, D. H. Leung, R. G. Bergman, K. N. Raymond, *Acc. Chem. Res.* **2005**, *38*, 351; b) T. S. Koblenz, J. Wassenaar, J. N. H. Reek, *Chem. Soc. Rev.* **2008**, *37*, 247.

[4] a) L. Que, W. B. Tolman, *Nature* **2008**, *455*; b) C. Di Nicola, Y. Yu. Karabach, A. M. Kirillov, M. Monari, L. Pandolfo, C. Pettinari, A. J. L. Pombeiro, *Inorg. Chem.* **2007**, *46*, 221; c) S. Chan, S. Yu, *Acc. Chem. Res.* **2008**, *41*, 969; d) G. Mezei, M. Rivera-Carrillo, R. G. Raptis, *Dalton Trans.* **2007**, 37.

[5] a) L. V. Tumanova, I. A. Tukhvatullin, D. S. Burbaev, R. I. Gvozdev, K. K. Andersson, *Russ. J. Bioorg. Chem.* **2008**, *34*, 177; b) A. S. Hakemian, A. C. Rosenzweig, *Annu. Rev. Biochem.* **2007**, *76*, 223; c) R. Lieberman, A. Rosenzweig, *Nature* **2005**, *434*, 177.

[6] Y. Shiota, K. Yoshizawa, *Inorg. Chem.* **2009**, *48*, 838.

[7] J. S. Woertink, P. J. Smeets, M. H. Groothaert, M. A. Vance, B. F. Sels, R. A. Schoonheydt, E. I. Solomon, *PNAS* **2009**, *106*, *45*, 18908.

[8] a) G. A. Olah, *Angew. Chem. Int. Ed.* **2005**, *44*, 2636; b) G. A. Olah, A. Goeppert, G. K. Surya Prakash, *Beyond Oil and Gas: The Methanol Economy*, Wiley-VCH, ISBN: 978–3-527–32422–4.

[9] a) P. Gamez, P. G. Aubel, W. L. Driessen, J. Reedijk, *Chem. Soc. Rev.* **2001**, *30*, 376; b) I. A. Koval, K. Selmeczi, C. Belle, C. Philouze, E. Saint-Aman, I. Gautier-Luneau, A. M. Schuitema, M. van Vliet, P. Gamez, O. Roubeau, M. Lüken, B. Krebs, M. Lutz, A. L. Spek, J.-L. Pierre, J. Reedijk, *Chem. Eur. J.* **2006**, *12*, 6138; c) S. Ferrer, E. Aznar, F. Lloret, A. Castineiras, M. Liu-Gonzalez, J. Borras, *Inorg. Chem.* **2007**, *46*, 372; d) A. E. Wendlandt, A. M. Suess, S. S. Stahl, *Angew. Chem. Int. Ed.* **2011**, *50*, 11062.

[10] a) K. Singh, J. R. Long, P. Stavropoulos, *Inorg. Chem.* **1998**, *37*, 1073; b) M. Casarin, C. Corvaja, C. di Nicola, D. Falcomer, L. Franco, M. Monari, L. Pandolfo, C. Pettinari, F. Piccinelli, P. Tagliatesta, *Inorg. Chem.* **2004**, *43*, 5865; c) C. Di Nicola, Y. Yu. Karabach, A. M. Kirillov, M. Monari, L. Pandolfo, C. Pettinari, A. J. L. Pombeiro, *Inorg. Chem.* **2007**, *46*, 221; d) G. A. Ardizzoia, S. Brenna, F. Castelli, S. Galli, C. Marelli, A. Maspero, *J. Organomet. Chem.* **2008**, *693*, 1870.

[11] a) G. A. Ardizzoia, S. Cenini, G. La Monica, N. Masciocchi, A. Maspero, M. Moret, *Inorg. Chem.* **1998**, *37*, 4284; b) M. Stollenz, M. John, H. Gehring, S. Dechert, C. Grosse, F. Meyer, *Inorg. Chem.* **2009**, *48*, 10049.

[12] a) H. V. R. Dias, H. V. K. Diyabalanage, M. G. Eldabaja, O. Elbjeirami, M. A. Rawashdeh-Omary, M. A. Omary, *J. Am. Chem. Soc.* **2005**, *127*, 7489; b) F. Gong, Q. Wang, J. Chen, Z. Yang, M. Liu, S. Li, G. Yang, *Inorg. Chem.* **2010**, *49*, 1658.

[13] M. Rivera-Carrillo, I. Chakraborty, G. Mezei, R. D. Webster, R. G. Raptis, *Inorg. Chem.* **2008**, *47*, 7644.

[14] a) F. Ramirez, S. B. Bhatia, A. V. Patwardhan, C. P. Smith, *J. Org. Chem.* **1967**, *32*, 2194; b) F. Ramirez, S. B. Bhatia, A. V. Patwardhan, C. P. Smith, *J. Org. Chem.* **1967**, *32*, 3547.

[15] a) T. Jin, Y. K. Hwang, D.-Y. Hong, S. H. Jhung, J.-S. Hwang, S.-E. Park, Y. H. Kim, J.-S. Chang, *Res. Chem. Intermed.* **2007**, *33*, 501; b) J. Y. Choi, J. Kim, S. H. Jhung, H.-K. Kim, J.-S. Chang, H. K. Chae, *Bull. Korean Chem. Soc.* **2006**, *27*, 10; c) Y. K. Hwang, J.-S. Chang, S.-E. Park, D. S. Kim, Y.-U. Kwon, S. H. Jhung, J.-S. Hwang, M. S. Park, *Angew. Chem. Int. Ed.* **2005**, *44*, 556.

[16] J.-P. Zhang, S. Kitagawa, *J. Am. Chem. Soc.* **2008**, *130*, 907.

[17] a) A. A. Mohamed, *Coord. Chem. Rev.* **2010**, *254*, 1918; b) H. V. R. Dias, H. V. K. Diyabalanage, M. G. Eldabaja, O. Elbjeirami, M. A. Rawashdeh-Omary, M. A. Omary, *J. Am. Chem. Soc.*

2005, *127*, 7489; c) H. V. R. Dias, H. V. K. Diyabalanage, *Polyhedron* **2006**, *25*, 1655; d) S. M. Tekarli, T. R. Cundari, M. A. Omary, *J. Am. Chem. Soc.* **2008**, *130*, 1669.
[18] A. L. Spek, *J. Appl. Crystallogr.* **2003**, *36*, 7.
[19] Quantachrome Autosorb, Version 1.56, **2009**.
[20] a) P. I. Ravikovitch, A. V. Neimark, *Colloids Surf.* **2001**, *187*, 11; b) S. J. Gregg, K. S. W. Sing, *Adsorption, Surface Area and Porosity*, London, Academic Press, UK, **1982**, p. 42.
[21] F. Rouquerol, J. Rouquerol, K. Sing, in *Adsorption by Powders and Porous Solids*, Academic Press, San Diego, **1999**.
[22] J. Jagiello, M. Thommes, *Carbon* **2004**, *42*, 1227.
[23] a) A. I. Cooper, M. J. Rosseinsky, *Nature Chem.* **2009**, 26; b) M. Bouchaour, N. Diaf, A. Ould-Abbas, M. Benosman, L. Merad, N.-E. Chabane-Sari, *Rev. Energ. Ren. ICPWE* **2003**, 99; c) H. Furukawa, N. Ko, Y. Bok Go, N. Aratani, S. Beom Choi, E. Choi, A. Ö. Yazaydin, R. Q. Snurr, M. O'Keeffe, J. Kim, O. M. Yaghi, *Science* **2010**, *329*, 424.
[24] L. Ma, A. Jin, Z. Xie, W. Lin, *Angew. Chem. Int. Ed.* **2009**, *48*, 9905.
[25] J. He, Y.-G. Yin, T. Wu, D. Li, X.-Ch. Huang, *Chem. Commun.* **2006**, 2845.
[26] P. C. Ford, E. Cariati, J. Burassa, *Chem. Rev.* **1999**, *99*, 3625.
[27] G.-F. Gao, M. Li, S.-Z. Zhan, Z. Lv, G.-h. Chen, D. Li, *Chem. Eur. J.* **2011**, *17*, 4113.
[28] A. B. P. Lever, *Inorganic Electronic Spectroscopy*, 2nd ed. Elsevier, New York, **1984**.
[29] G. M. Sheldrick, *SHELXL-97*, Program for Refinement of Crystal Structures, University of Göttingen, Germany, **1997**.
[30] Oxford Diffraction, CrysAlis Pro rel. C171.33.48, **2009**.
[31] A. Altomare, M. C. Burla, M. Camalli, G. L. Cascarano, C. Giacovazzo, A. Guagliardi, A. G. G. Moliterni, G. Polidori, R. Spagna, *J. Appl. Crystallogr.* **1999**, *32*, 115.